International Journal of Research in Engineering and Innovation (IJREI)
journal home page: http://www.ijrei.com
ISSN (Online): 2456-6934

Numerical simulation model of solar air heater using ansys-14

Radha Kant[1*], Akhilesh Kumar Singh[2], Sumit Chawla[3]

[1]*Assistant Professor, Department of Mechanical Engineering, Delhi Technical Campus, Greater Noida Uttar Pradesh -201308, India.*
[*]*Email address: mradhakant07@gmail.com, Tel: +91-9816926542.*
[2]*Assistant Engineering Manager, L& T Construction, EDRC-HQ Manpkkam, Chennai-600089*
[3]*Assistant Professor, Department of Mechanical Engineering, Delhi Technical Campus, Greater Noida Uttar Pradesh -201308, India.*

Abstract

Thermal performance of downward- type single-pass flat plate solar air heater (SAH) with pin fins attached on absorber plate are investigated numerically. Calculations of outlet air temperature and collector efficiency have been done with and without application of recycling operation. Numerical simulation of solar air heater has been performed by the use of ANSYS-14 (FLUENT) software. 196 square pin fins on absorber plate has been attached and by maintaining both the pitch lengths (transverse and longitudinal) constant optimization of fin height and thickness (side) has been done for various values mass flow rates and results are represented in graphical as well as tabular form. The effects of in-line and staggered arrangements of fins on the performances of solar heater have been compared. It is found that due to application of pin fins, with a mass flow rate of 0.02 kg/s, thermal efficiency of solar air heater increases upto 99% and 91% for staggered and in-line arrangements respectively, as compared to SAH operating without fins with same air flow rate. The results showed that SAH with staggered arrangement is upto 13%, 6.5% and 4.5% more efficient than in-line arrangement with a mass flow rates 0.05, 0.01, 0.02 kg/s respectively.

Keywords: solar air heater, pin fins, ANSYS-14

1. Introduction

Man has needed and used energy at an increasing rate for his sustenance and well-being ever since he came on the earth a few million years ago. Primitive man required energy primarily in the form of food. He derived this by eating plants or animals which he haunted. Subsequently he discovered fire and his energy needs increased as he started to make use of wood and other biomass to supply the energy needs for cooking as well as for keeping himself warm. With the passage of time, man started to cultivate land for agriculture. He added a new dimension to the use of energy by domesticating and training animals to work for him. With further demand for energy, man began to use the wind for sailing ships and for driving windmills, and the force of falling water to turn water wheels. Till this time, it would not be wrong to say that the sun was supplying all the energy needs of man either directly or indirectly.

The industrial revolution which began with the discovery of the steam engine (AD1700) brought about a great many changes. For the first time, man began to use a new source of energy, viz. coal, in large quantities. A little later, the internal combustion engine was invented (AD 1870) and the other fossil fuels, oil and natural gas began to be used extensively. The invention of heat engines and use of fossil fuels made energy portable and introduced the much needed flexibility in man's movement. For first time, man could get the power of a machine where he required it and was not restricted to a specific site like a fast-running stream for running a water wheel or a windy hill for operating a windmill. This flexibility was enhanced with the discovery of electricity and the development of central power generating stations using either fossil fuels or water. A new source of energy-nuclear energy- came on the scene after the Second World War. The first large nuclear power station was commissioned about 70 years ago and now these days, nuclear energy is providing a significant

Corresponding author: Radha Kant
Email Address:mradhakant07@gmail.com

amount of the energy requirements of many countries.

- The production oil reached a maximum around 1985 and now is declining. Present indications are that most of the reserves of oil and natural gas are likely to be consumed in other 40 year.
- As oil and natural gas become scarcer, a greater emphasis will fall on coal. It is likely that the production of coal will touch a maximum somewhere between the years 2030 and 2060 and that 80 per cent of the amount available could consumed by 2250 AD.

1.1 Introduction to solar air heater with recycle

It is a particular type of solar air heater in which some amount of heated air from the outlet of air heater is continuously circulated through recycle channel and it is re-mixed to the fresh air at the inlet. Due to recycling the temperature and flow rate of air get increased at inlet. The ratio of rate at which air is circulated through recycle channel to the rates at which air is collected at outlet is called recycle ratio or reflux ratio (R). A schematic diagram of recycle type solar air heater is shown in fig.1.
It was pointed out that applications of the recycle effect in the design and operation of the equipment with external or internal reflux can effectively enhance the effect on heat- and mass-transfer, leading to improved performance [5-8]. Actually, there are two conflict effects of recycle operation. One is the desirable effect of increasing fluid velocity, resulting in enhancement of convective heat- or mass-transfer, while the other is the undesirable effect of decreasing the driving force (temperature or concentration difference) due to remixing. It was found that the increase in convective heat- or mass-transfer by increasing the reflux ratio can generally compensate for the decrease of driving force, leading to improved performance.

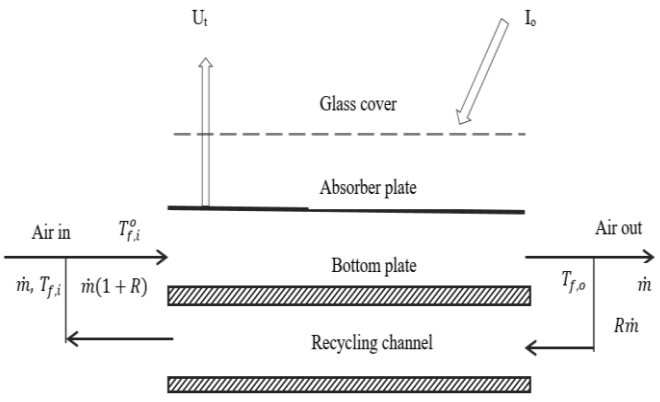

Figure: 1 Schematic diagram of solar air heater with recycle

2. Literature Review

Norris and Spofford [9], derived first basic heat transfer and flow-friction data for pin fin surfaces. The experiments were carried out with the aim of the derivation of basic parameters of forced convection heat transfer for continuous, corrugated, strip and pin fins. By use of the perimeter as the length scale, they could approximately represent the heat transfer data with a single curve for a single plane, single cylinder, various strip fins and pin fins. Norris and Spofford included in their tests an in-line pin fin arrangement with pin diameters of 0.5 mm and 1 mm and a pin length of ~ 19 mm.

Kays [10], performed probably the most extensive study of pin fins as elements for heat transfer enhancement. He presented test data for four in-line pin arrangements and one staggered arrangement. It was demonstrated that owing to a high area to perimeter ratio, pin fins provide one method for obtaining very high heat transfer coefficients while at the same time maintaining high fin effectiveness. He concluded that despite high friction factors of pin fin surfaces, it is possible to design heat exchangers that are competitive, from volume and weight points of view, with heat exchangers having continuous or louvered fins.

Theoclitus[11], performed a limited parametric study of pin fins with an in-line arrangement. He investigated nine different geometries of in-line pin fins with circular cross-section with length to diameter ratios in the range$4 \leq l/d \leq 12$. Further, he investigated the acoustic and vibrational characteristics of the flow over the pins and concluded that these phenomena are basically influenced by the fluid velocity and heat exchanger configuration. In general, the average heat transfer rates reported by Theocritus were lower for short than for longer cylinders.

Sparrow and Ramsey [12], reported excellent experimental work on the influence of tip clearance for a staggered wall-attached array of cylinders. They obtained data on heat transfer coefficients by applying the analogy between heat and mass transfer via the naphthalene sublimation technique. They found that the heat transfer coefficient increases moderately as the length of the cylinder increases and the tip clearance between the pin and the shroud decreases. On the other hand, the array pressure drop increases markedly with increasing cylinder length. This behavior was explained with inter-cylinder velocities for short pins which are less than the mean velocity, whereas for taller cylinders the inter-cylinder velocities tend to approach the mean value.

VanFossen [13], investigated the heat transfer from short pin fin arrays taking into account the heat transfer from the pin fin surfaces and from end walls. He found that heat transfer from short pins with a length to diameter ratio l/d = 2 and 0.5 was lower than those of long pins based on the available data for long pins. Further he found that heat transfer from the pin surface was 35% higher than from the end walls.

Sparrow and Molki [14], investigated the effect of missing a pin in the array on the heat transfer and pressure drop characteristics for the flow over pin fins.

Metzger et al. [15], in their investigations of short pin fin arrays with l/d = 1, found the pin surface heat transfer coefficients to be approximately twice as large as those

acting on the end walls. The main objective of the investigations was the influence of the array orientation with respect to the mean flow direction on the heat transfer rates and the associated pressure losses for circular and oblong pin fin arrays. It was reported that with circular pin fins rotated two-thirds of the way towards a in-line orientation from a staggered orientation, a 9% increase in heat transfer and an18% decrease in pressure loss were observed. For the oblong pins there was 20 % increase in heat transfer compared with the circular pin fin arrays but this increase was offset by an approximately 100% increase in pressure loss.

Babus'Haq et al. [16] studied the influences of the pin fin distance and the pin fin material on thermal performance of the inline and staggered pin fin assembly. They determined the optimal fin distance in the stream wise direction for a uniform span wise distance and noted that the optimal spacing increases as the thermal conductivity of the pin fin material increases. Further, they noted that the overall pressure drop for all tested configurations increases steadily with increasing mean inlet velocity and with decreasing uniform pin fin spacing

3. Numerical simulation and analysis

Numerical Simulation in a crude sense is the method of predicting the output of a proposed system or an existing system without conducting experiment on it. A commercially available software ANSYS-14.0 (FLUENT) is used to investigate the thermal performance of solar air heater with pin fins attached on absorber plate.

3.1 Steps for Simulation in Computer Aided Engineering Software (CAE)

Simulation in CAE software contains three main steps and various sub-steps

(a) Pre-Processing

This is the first step of CFD simulation process, which helps in describing the geometry in the best possible manner. It has some sub-steps as follows

- Generation of geometry
- Grid generation
- Physics model selection
- Material properties
- Boundary condition
- Initial condition

(b) Solver

Once the problem physics has been identified, fluid material properties, flow physics model, and boundary conditions are set to solve using computer through following processes

- Solver selection
- Residual target
- Initialization

(c) Post Processing

The next step after getting the results is to analyze the results with different methods like contour plots, stream lines, vector plots etc.

3.1.1 Geometry Generation

The collector consists of one glass cover (2 mm thickness), a black absorber plate (0.6 x 0.6 m), 196 square shape pin fins of aluminum attached on absorber plate, one channel of dimensions (0.6 x 0.6x 0.05 m) for downward flow of air and an insulated recycle channel of same dimensions as shown in fig. 2. The air flows in passage between glass cover and absorber plate and some amounts of hot air from outlet is re-circulated through recycle channel and it is re-mixed with cold air at inlet of SAH.

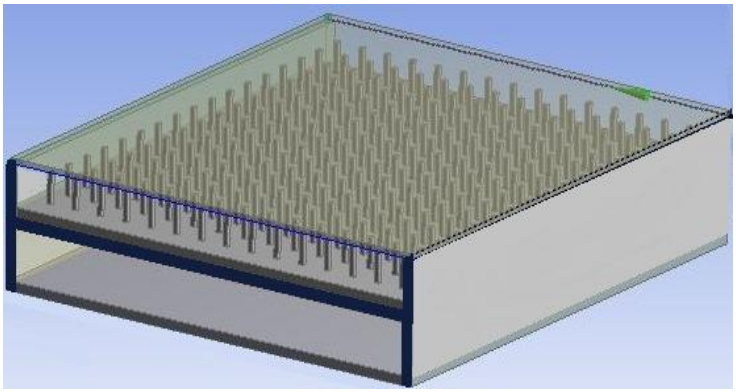

(a)

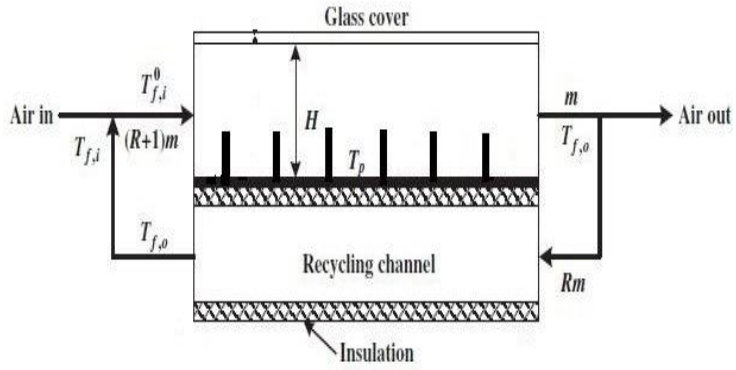

(b)

Figure: 2 (a) Recycle type solar air heater with pin fins attached (b) Schematic diagram of solar air heater

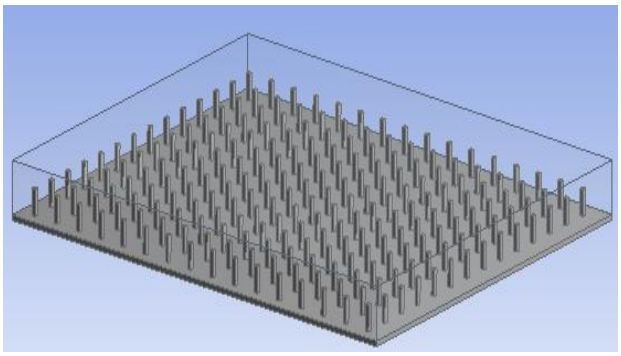

Figure: 3 Computational domain of SAH

4. Governing Equations

The governing transport equations in 3D Cartesian coordinates for the fluid flow, heat and mass transfer are given below

Continuity equation

$$\frac{\partial u}{\partial x}+\frac{\partial v}{\partial y}+\frac{\partial w}{\partial z}=0 \quad (1)$$

X- Momentum equation

$$u\frac{\partial u}{\partial x}+v\frac{\partial u}{\partial y}+w\frac{\partial u}{\partial z}=-\frac{1}{\rho}\frac{\partial p}{\partial x}+\nu\left[\frac{\partial^2 u}{\partial x^2}+\frac{\partial^2 u}{\partial y^2}+\frac{\partial^2 u}{\partial z^2}\right] \quad (2)$$

Y- Momentum equation

$$u\frac{\partial v}{\partial x}+v\frac{\partial v}{\partial y}+w\frac{\partial v}{\partial z}=-\frac{1}{\rho}\frac{\partial p}{\partial y}+\nu\left[\frac{\partial^2 v}{\partial x^2}+\frac{\partial^2 v}{\partial y^2}+\frac{\partial^2 v}{\partial z^2}\right] \quad (3)$$

Z Momentum equation

$$u\frac{\partial w}{\partial x}+v\frac{\partial w}{\partial y}+w\frac{\partial w}{\partial z}=-\frac{1}{\rho}\frac{\partial p}{\partial z}+\nu\left[\frac{\partial^2 w}{\partial x^2}+\frac{\partial^2 w}{\partial y^2}+\frac{\partial^2 w}{\partial z^2}\right] \quad (4)$$

Energy equation

$$u\frac{\partial T}{\partial x}+v\frac{\partial T}{\partial y}+w\frac{\partial T}{\partial z}=\alpha\left[\frac{\partial^2 u}{\partial x^2}+\frac{\partial^2 u}{\partial y^2}+\frac{\partial^2 u}{\partial z^2}\right] \quad (5)$$

In the above equations, u, v and w are the velocity components in x, y and z directions, p and T are the pressure and temperature of the flowing air.

Transport equation for the Realizable *k-ε* model.

Turbulent kinetic energy *k* equation

$$\frac{\partial}{\partial t}(\rho\varepsilon)+\frac{\partial}{\partial x_j}(\rho k u_j)=\frac{\partial}{\partial x_j}\left[\left(\mu+\frac{\mu_t}{\sigma_k}\right)\frac{\partial k}{\partial x_j}\right]+G_k+G_b-\rho\varepsilon-Y_M+S_k \quad (6)$$

Rate of energy dissipation ε equation,

$$\frac{\partial}{\partial t}(\rho\varepsilon)+\frac{\partial}{\partial x_j}(\rho\varepsilon u_j)=\frac{\partial}{\partial x_j}\left[\left(\mu+\frac{\mu_t}{\sigma_\varepsilon}\right)\frac{\partial \varepsilon}{\partial}\right]+\rho C_1 S\varepsilon-\rho C_2\frac{\varepsilon^2}{k+\sqrt{\nu\varepsilon}}+C_{1\varepsilon}\frac{\varepsilon}{k}c_{3\varepsilon}G_b+S_\varepsilon \quad (7)$$

Where, $c_1=max\left[0.43,\frac{\eta}{\eta+5}\right]$, $\eta=S\frac{k}{\varepsilon}$, $s=\sqrt{2s_{i,j}s_{i,j}}$ (8)

In these equations, G_k represents the generation of turbulence kinetic energy due to themean velocity gradients, G_b is the turbulence kinetic energy generated due to buoyancy, Y_M represents the contribution of the fluctuating dilatation in compressible turbulence to the overall dissipation rate, C_2 and $C_{1\varepsilon}$ are the constant, σ_k and σ_ε are theturbulent Prandtl numbers for k and ε, respectively. S_k and S_ε are user-defined source terms.
The eddy viscosity is computed from

$$\mu_t=\rho C_\mu\frac{k^2}{\varepsilon} \quad (9)$$

The model constants are $C_{1\varepsilon}=1.44, C_2=1.9, \sigma_\varepsilon=1.2$ (10)

Table: 1 properties of materials

Material	Density (kg/ m^3)	Specific heat J/kg K	Thermal Conductivity (W/m ^{2}K)	Refractive index
Air	1.225	1006	0.0242	--
Glass	2600	840	1.05	1.5
Aluminum	2719	871	202.4	--

5. Boundary Conditions

5.1 Boundary Conditions without Recycling

(a) Inlet boundary: At the inlet of SAH uniform mass flow rates are used and the direction is normal to the opening at inlet, mass flow rates along the x-axis are taken as 0.005, 0.01, 0.015 and .02 kg/s. Turbulence parameters at the inlet are defined using turbulence intensity (assuming 5%) and inlet characteristic length (hydraulic diameter) as 0.0923 m. Inlet air temperature is taken as 288 K

(b) Both the radiation and convection boundary conditions are applied to the glass cover. Convective heat transfer coefficient (h_w) for ambient air flowing over the outside surface of the glass cover depends primarily on the wind velocity.

$$h_w = 5.7 + 3.8\ V \quad (11)$$

Ambient temperature for radiation from top of glass is taken as 283 K.

(c) Absorber plate is assumed to be insulated at bottom side.
(d) Sides and bottom losses are assumed to be zero.
(e) Boundary condition at outlet is taken as pressure outlet.

5.2 Boundary condition with recycle operation

(a) Inlet boundry conditions

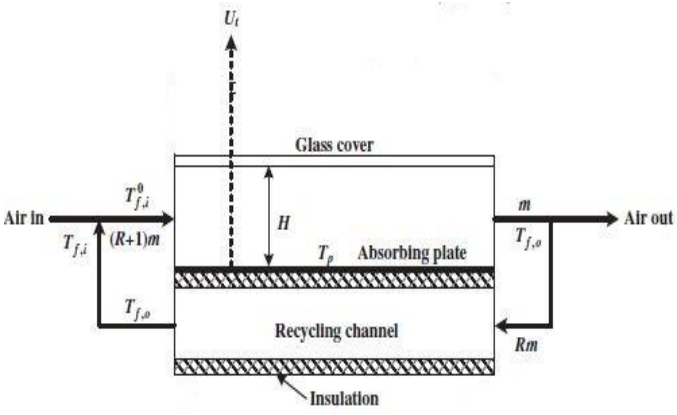

Figure: 4 schematic diagram of solar air heater operating with recycle

In order to determine the mixed air temperature $T^o_{f,i}$ because of recycling, let take an energy balance at the inlet with the inlet temperature $T_{f,i}$ as the reference temperature.

$$\dot{m}C_p(T_{f,i} - T_{f,i}) + \dot{m}RC_p(T_{f,o} - T_{f,i}) = \dot{m}(1 + R)C_p(T^o_{f,i} - T_{f,i}) \quad (12)$$

$$T^o_{f,i} = T_{f,i} + \left[\frac{R}{1+R}\right](T_{f,o} - T_{f,i}) \quad (13)$$

Hence in case of recycling uniform air flow rate at inlet is taken as $\dot{m}(1 + R)$ instead of $\dot{m}$ and inlet air temperature is given by equation 3.16.
b) Recycle channel is assumed to be perfectly insulated.
While all other boundary conditions are same as without recycling.

5.3 Solver selection

There are two technologies are available in ANSYS Fluent to solve any problem one is pressure based solver and another is density based solver here in this study pressure based solver is used for Solar Air Heater simulation, Two algorithms also exist under the pressure-based solver, a segregated algorithm and a coupled algorithm, for present work coupled algorithm is used in which the momentum equations and the pressure-based continuity equation are solved in a coupled manner. Also the coupled algorithm significantly improves the convergence speed over the segregated algorithm. The coupled algorithm solves the momentum and pressure-based continuity equations together. The full implicit coupling is achieved through an implicit discretization of pressure gradient terms in the momentum equations, and an implicit discretization of the face mass flux, including the Rhie-Chow pressure dissipation terms.

5.4 Initialization

Before we start our calculations or patch initial values for selected variables in selected cells we must initialize the flow field in the entire domain. The Solution Initialization Task Page allows us to set initial values for the flow variables and initialize the solution using these values. Initialization will result in the volume fraction, X, Y, and Z velocities, and pressure being patched in the domain. The volume fraction will be patched in the domain based on the free surface level of the selected zone from the Compute from list. The velocities in the domain will be patched assuming the constant value provided for the velocity magnitude in the selected zone. There are two types of initialization method.

- Hybrid Initialization
- Standard Initialization

5.5 Hybrid Initialization

It is a collection of boundary interpolation methods, where variables, such as temperature, turbulence, species fractions, volume fractions, etc., are automatically patched based on domain averaged values or a particular interpolation recipe. We have to proceed through following three steps in using hybrid initialization.
Number of Iterations uses a default value of 10. This is the number of iterations that will be performed while solving the Laplace equations to initialize the velocity and pressure. In general we do not need to change the number of iterations. However, for complex and highly curved geometries, if the default number of iterations is not enough to reach the convergence tolerance of 1e-06 and the flow fields are not to our liking, then we have to increase the number of iterations and re-initialize the flow.

5.6 Explicit Under-Relaxation

Factor uses a default value of 1. This value will be used while solving the Laplace equation to initialize the velocity and pressure. In general, we do not need to change the explicit under-relaxation factor. However, for some cases, where the scalar residuals are oscillating and showing difficulty reaching the convergence tolerance of 1e-06, we have to re-initialize the flow by reducing the under-relaxation factor. We may also want to increase the number of iterations to produce a smooth initialization field for the velocity and pressure.
Reference Frame is set to Relative to Cell Zone by default.

If our problem involves moving reference frames or sliding meshes, indicate whether the initial velocities are absolute velocities or velocities relative to the motion of each cell zone by selecting absolute or Relative to Cell Zone. If no zone motion occurs in the problem, the two options are equivalent. If the solution in most of our domain is rotating, using the relative option may be better than using the absolute option.

5.7 Standard Initialization

Allows us to define values for flow variables and initialize the flow field to these values. We can compute the values from information in a specified zone, enter them manually, or have the solver compute average values based on all zones. We can also indicate whether the specified values for velocities are absolute or relative to the velocity in each cell zone. The steps for standard initialization are as follows

Compute from is a drop-down list of zones; the default values for applicable variables will be computed from information contained in the zone that we select from this list. The computation will occur when we select the required zone, and the variable values will be displayed in Initial Values. We can also choose the all zones item in this list to compute average values based on all zones.

Reference Frame indicates whether the initial velocities are absolute velocities (Absolute) or velocities relative to the motion of each cell zone (Relative to Cell Zone). This selection is necessary only if our problem involves moving reference frames or sliding meshes. If there is no zone motion, both options are equivalent.

Initial Values displays the initial values of applicable variables. We can use Compute from to compute values from a particular zone, or we can enter values directly.

Initialize initializes the entire flow field to the values listed.

Reset resets the fields to their "saved" values.

Standard initialization is used for simulation of solar air heater. The values are computed from inlet and fluid is used as a reference frame.

5.8 Calculation for collector efficiency

By the application of above processes we get outlet air temperature, mean fluid temperature, glass cover temperature and mean absorber plate temperature. After getting the outlet air temperature we predict the thermal efficiency of solar collector by the use of following equations.

$$\eta = \frac{Useful\ gain\ of\ energy\ carried\ away\ by\ air}{Total\ solar\ radiation\ incident}$$

$$= \frac{\dot{m} C_p (T_{f,o} - T_{f,i})}{I_o A_c} \qquad (14)$$

and for recycling,

$$\eta = \frac{\dot{m}(1+R) C_p (T_{f,o} - T^o_{f,i})}{I_o A_c} \qquad (15)$$

Where mixed air flow temperature $T^o_{f.i}$ at beginning of the upper channel, can be calculated by using equation (13).

6. Results and discussions

Four inlet mass flow rates of 0.005, 0.01, 0.015, and 0.02 kg/s corresponding to the *Re* number to be 850, 1670, 2500 and 3400 are adopted to analyze the thermal performance of a flat plate solar air heater with internal pin fins attached by operating with external recycle. At the absorber plate, square pin fins are arranged in line and staggered ways. Both staggered and in-line cases are investigated and the results are compared and analyzed for the following design and operating conditions:

$L = B = 0.6$ m; $A_c = LB = 0.36$ m^2; $\tau = 0.90$; $\alpha_p = 0.95$; $\varepsilon_g = \varepsilon_p = 0.95$; $I_o = 830$ w/m^2; $T_{f,i} = 288$ K; $V = 1$ m/s; $T_a = 283$ K; $\sigma = 5.67 \times 10^{-8}$ w/m^{2}K^4; N=196.

Table: 2 Variations of outlet temperature with fins height and thickness

m (kg/s)	h(mm)	t=5 mm	t=10 mm	t=15 mm	t=20 mm	t=25 mm	t=30 mm
		$T_{f,o}$ (K)	$T_{f,o}$ (K)	$T_{f,o}$ (K)	$T_{f.o}$ (K)	$T_{f.o}$ (K)	$T_{f,o}$ (K)
0.005	0	300.52	300.52	300.52	300.52	300.52	300.52
	5	301.95	302.44	302.60	302.53	302.05	301.57
	10	303.05	304.10	304.18	304.11	303.48	302.47
	15	304.10	305.48	305.52	305.52	304.80	303.32
	20	305.03	306.68	306.70	306.51	305.90	304.07
	25	305.95	307.78	307.74	307.53	306.70	304.85
	30	306.83	309.26	309.24	309.10	307.40	305.26
	35	307.40	309.66	309.70	309.60	307.95	305.56
	40	307.83	309.92	309.90	309.85	308.36	305.53
	45	308.07	310.15	310.13	310.00	308.31	305.46
0.01	0	295.85	295.85	295.85	295.85	295.85	295.85
	5	296.25	297.32	298.02	298.25	297.60	297.08
	10	297.85	298.82	299.35	299.55	299.40	298.6
	15	299.08	299.90	300.55	300.85	300.55	300.26
	20	300.02	300.80	301.42	302.00	301.52	301.15
	25	300.23	301.52	302.25	302.72	302.15	301.45
	30	300.42	301.65	302.58	302.74	302.05	301.28
	35	300.55	301.76	302.56	302.64	301.85	301.14
	40	300.65	301.84	302.51	302.50	301.54	301.03
	45	300.68	301.87	302.46	302.21	301.35	300.85
0.02	0	293.13	293.13	293.13	293.13	293.13	293.13
	5	293.95	294.49	294.95	295.45	295.90	295.70
	10	294.78	295.31	295.72	296.25	296.60	296.02
	15	295.62	296.10	296.40	296.78	297.03	296.66
	20	295.73	296.25	296.67	297.05	297.23	296.75
	25	295.81	296.38	296.96	297.55	297.85	297.10
	30	295.85	296.45	296.94	297.48	297.80	297.03
	35	295.91	296.27	296.65	297.36	297.60	296.90
	40	295.86	296.18	296.56	297.18	297.43	296.75
	45	295.74	296.16	296.45	297.01	297.20	296.55

As thickness of fins increases, the air temperature is firstly increased due to increase in exposed surface area for convective heat transfer but simultaneously causes for decrease in plate area available for absorbing the sun radiation. Hence after reaching a particular optimum value of fin thickness second effect is dominated and thereafter temperature of air get decreased continuously as indicated from table 2.

6.1 Velocity vectors, temperature contours and stream lines

Velocity vectors, temperature contours and stream lines were generated in ANSYS-14(FLUENT) software and are shown in fig. 5-12.

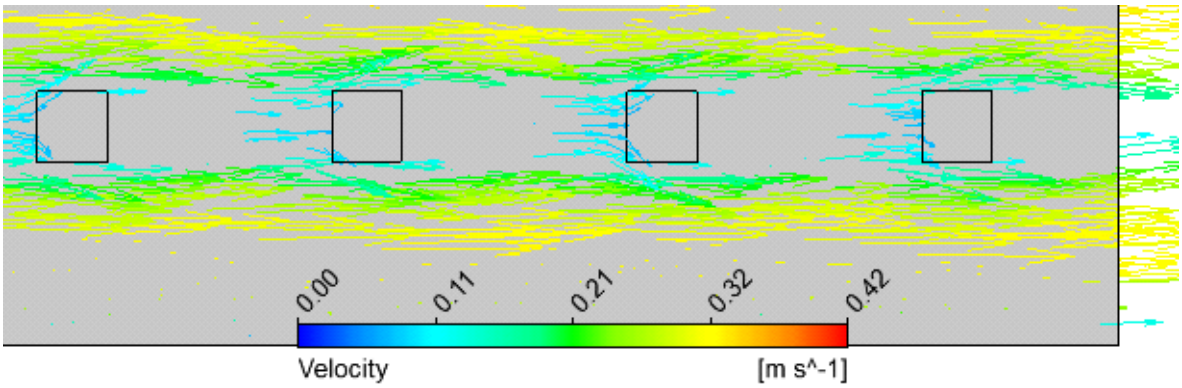

Figure: 5 Velocity vector 1 generated in ANSYS-14

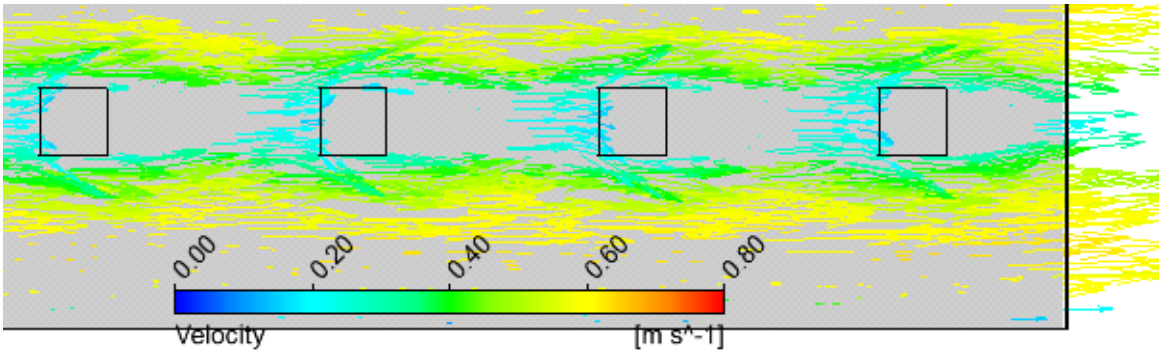

Figure: 6 Velocity vector 2 generated in ANSYS-14

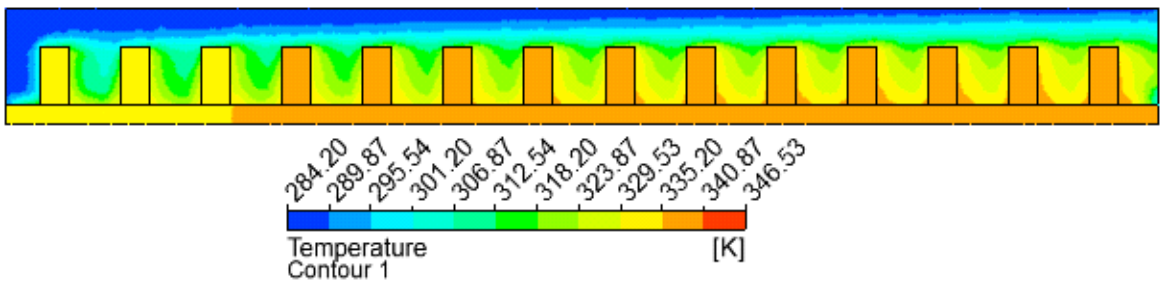

Figure: 7 Temperature Contour 1 (a) generated in ANSYS-14

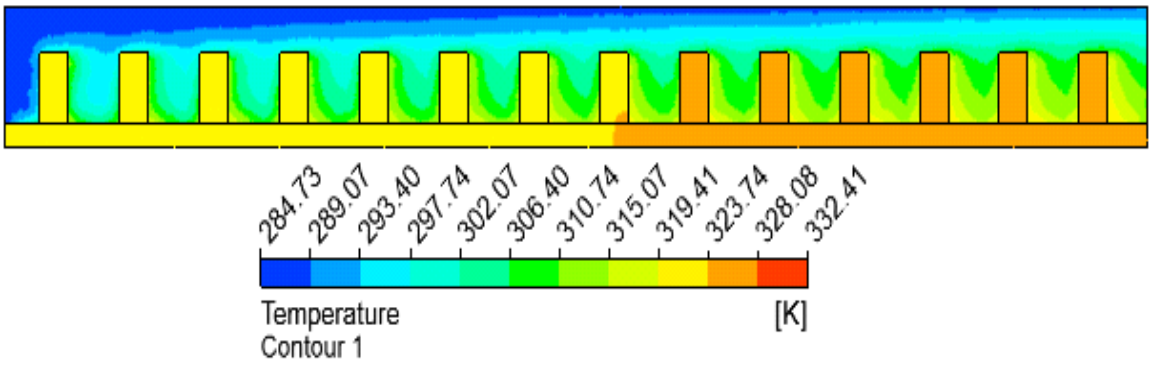

Figure: 8 Temperature Contour 1 (b) generated in ANSYS-14

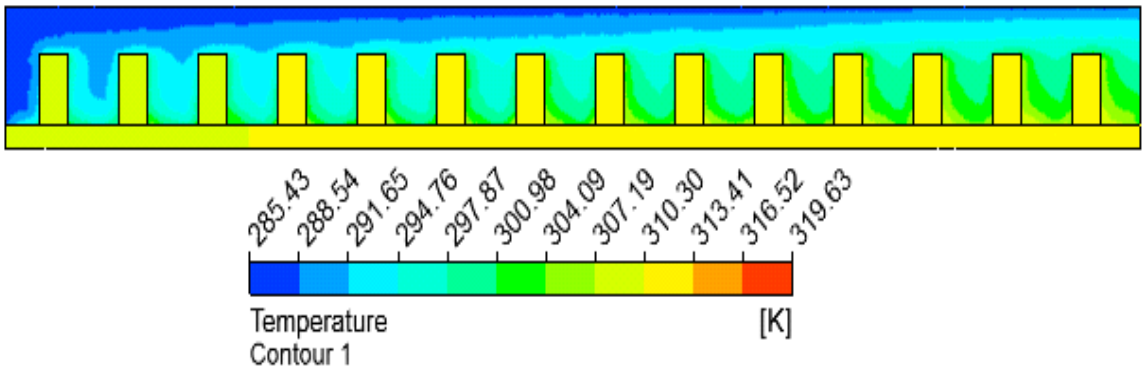

Figure: 9 Temperature Contour 1 (c) generated in ANSYS-14

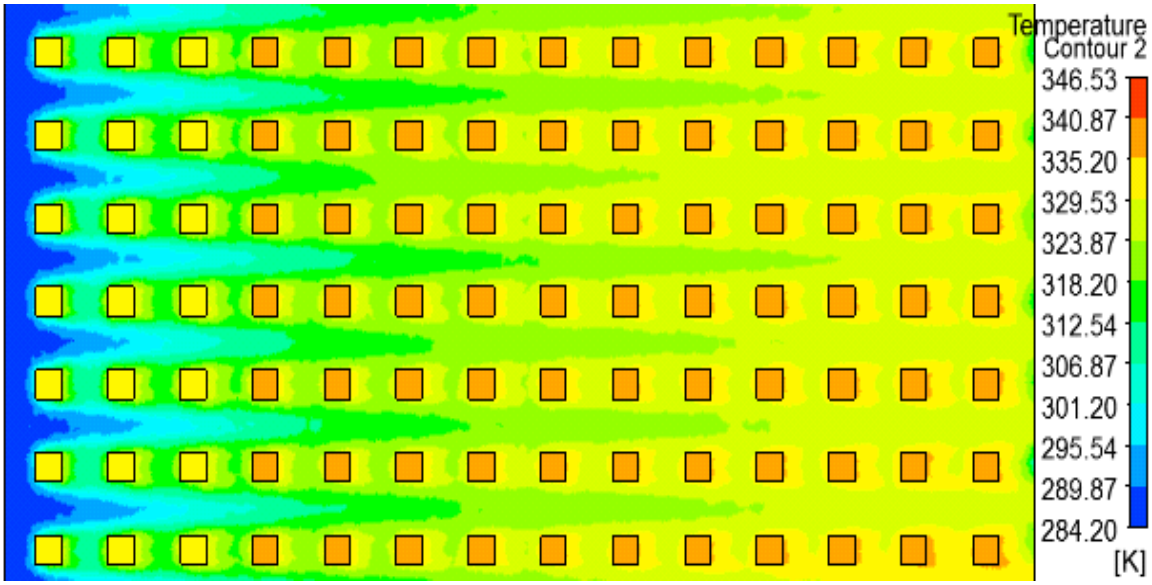

Figure: 10 Temperature Contour 2 at z-x plane, from y=20 mm, for m=0.005 kg/s

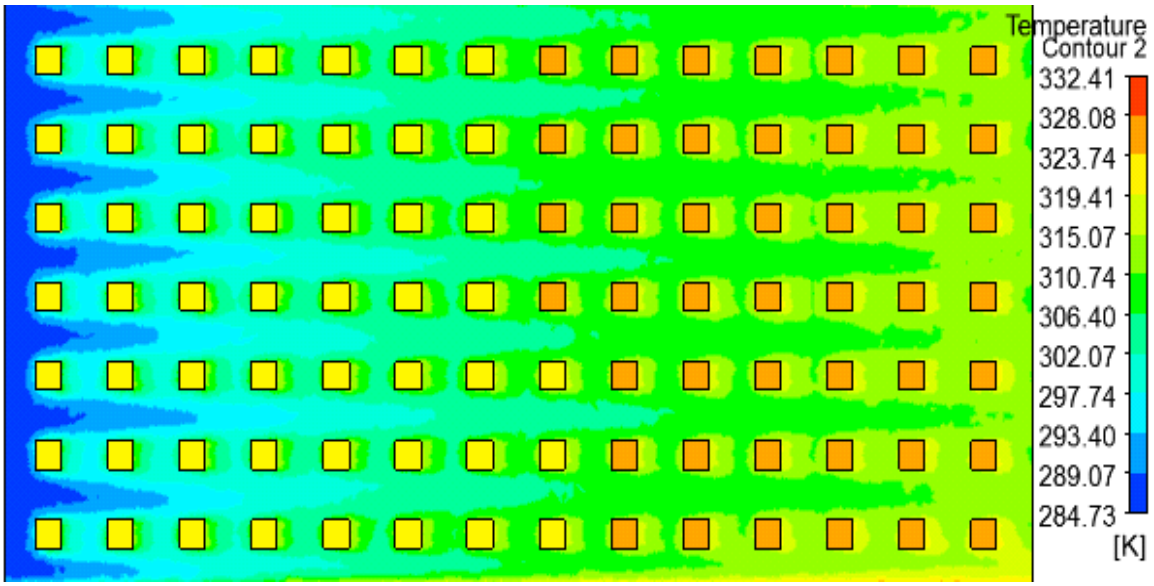

Figure: 11 Temperature Contour 2 at z-x plane, from y=20 mm, for m=0.01 kg/s

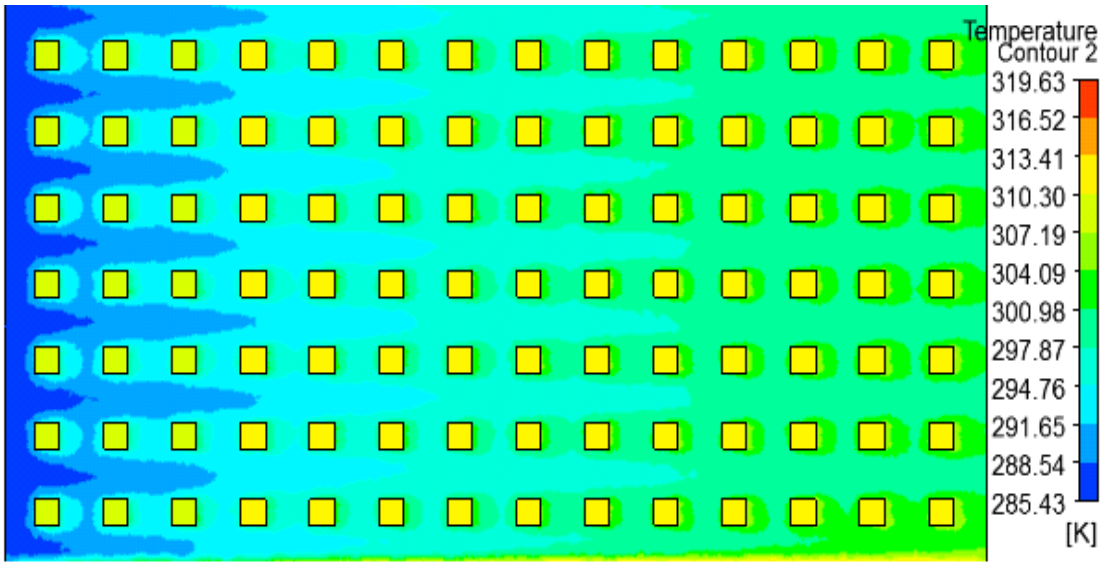

Figure: 12 Temperature Contour 2 at z-x plane, from y=20 mm, for m=0.02 kg/s

For lower air flow rates mean temperature of absorber plate and fins is higher than that of high flow rates, as indicated from figs. 7-9. The temperature variations at z-x plane and from a distance y = 20 mm are shown in fig 10-12. Since for low air flow rates (0.005 kg/s) energy carried away by fluid is lower compare to higher flow rates (0.02 kg/s). That's why the mean temperature of absorber plate and fins is highest for air flow rate of 0.005 kg/s and lowest for flow rate of 0.02 kg/s, as shown in fig 10-12.

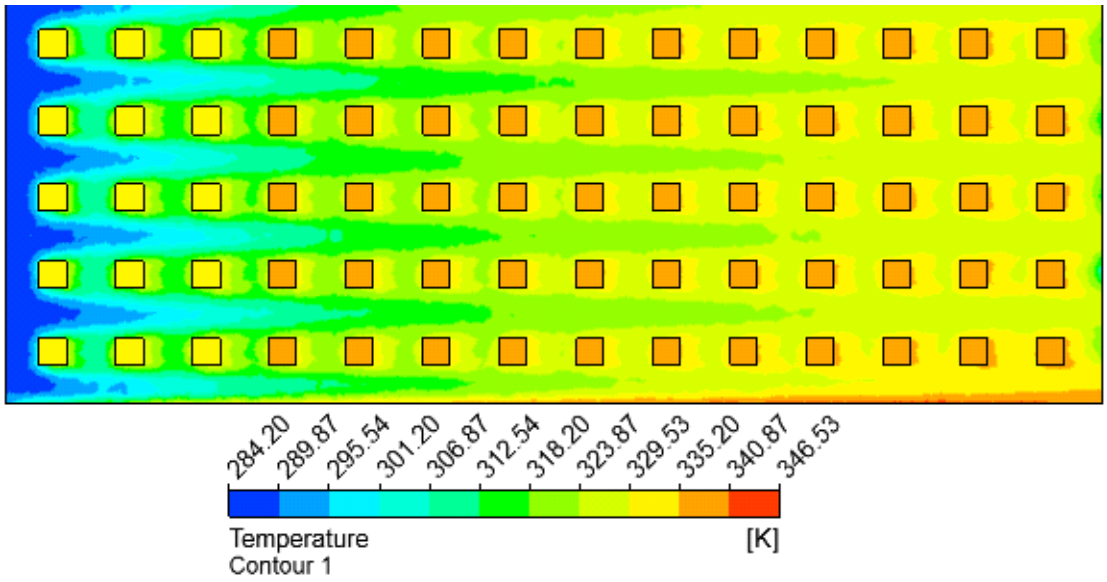

Figure: 13 Comparison Temperature variations at z-x plan for m=0.005 kg/s (in-line arrangement)

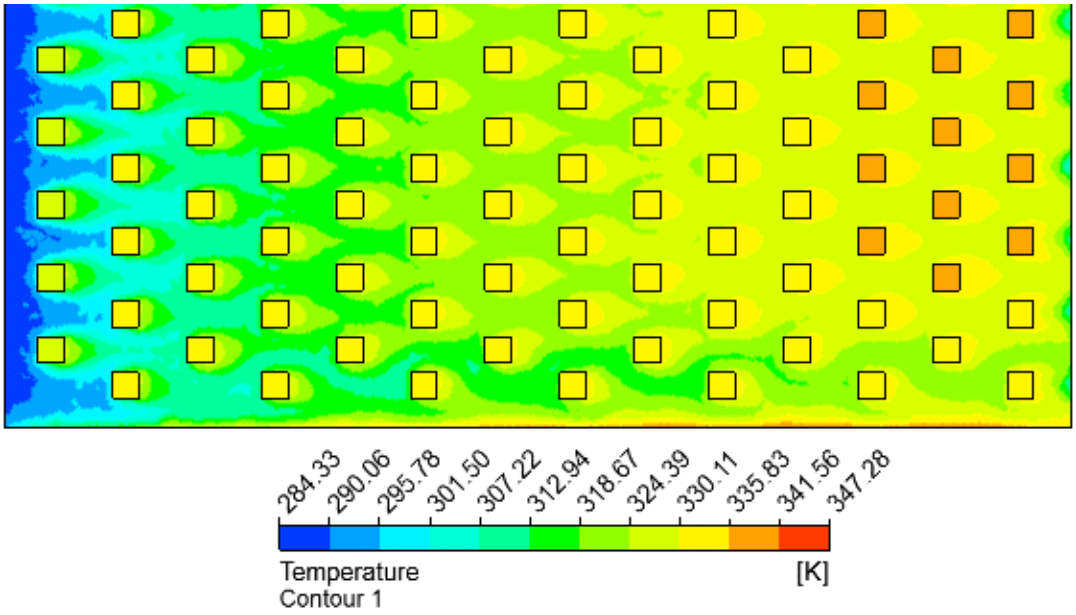

Figure: 14 Comparison Temperature variations at z-x plan for m=0.005 kg/s (staggered arrangement)

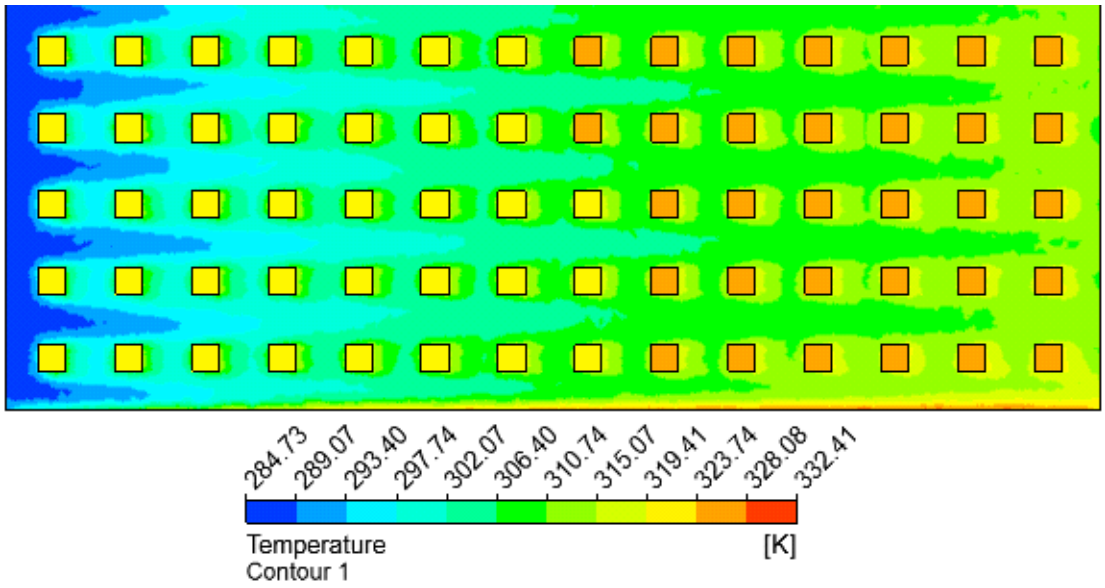

Figure: 15 Comparison temperature variations at z-x plan for m=0.001 kg/s (in-line arrangement)

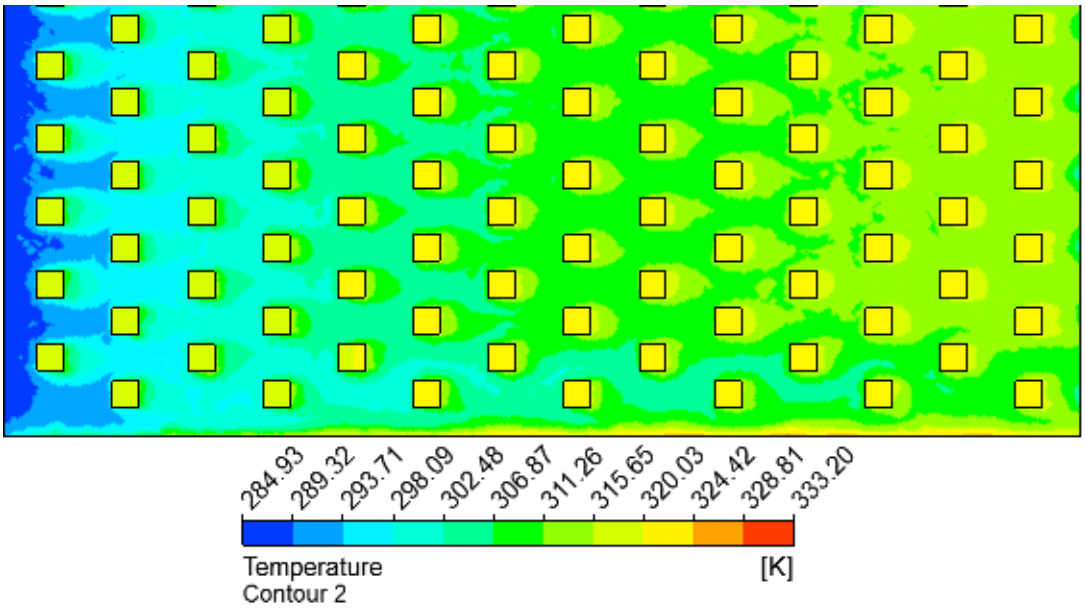

Figure: 16 Comparison temperature variations at z-x plan for m=0.001 kg/s (staggered arrangement)

Fig. 13 &14 show the temperature variations for in-line arrangement and staggered arrangement respectively with mass flow rate of 0.005 kg/s. And fig. 15 & 16 show the temperature variations for in-line arrangement and staggered arrangement respectively with mass flow rate of 0.01 kg/s. since energy transfer to the air is more for staggered arrangement that's why mean temperature of fins seems lower than in-line arrangement. Since at lower air flow rates, air has more time of contact with absorber plate and fins that is why at lower mass flow rates temperatures of air are found to be higher than temperatures of air at higher flow rates.

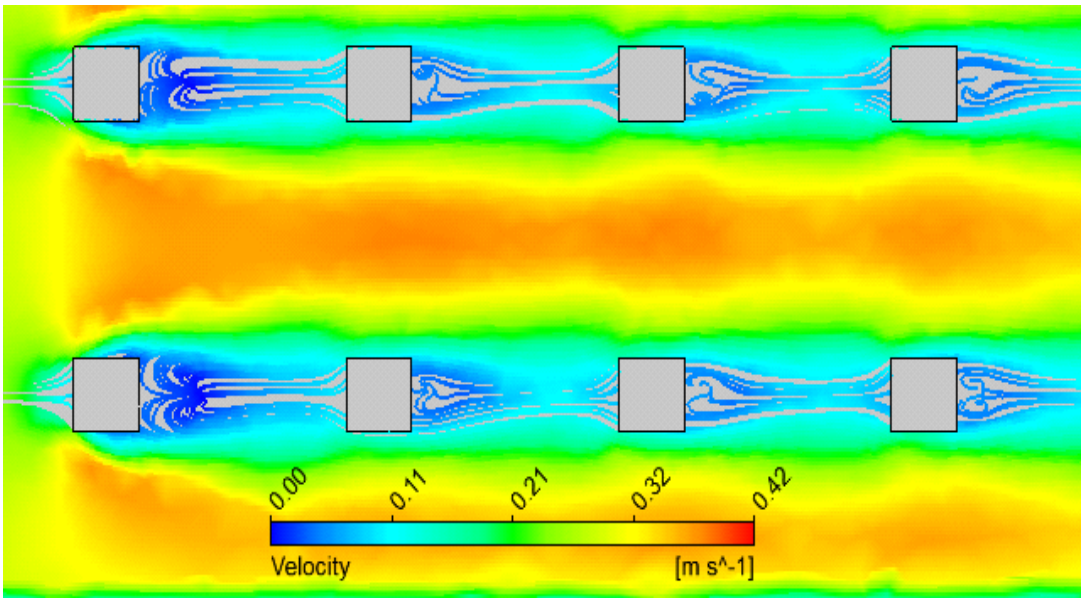

Figure: 17 Stream lines for m=0.01 kg/s (in-line arrangements)

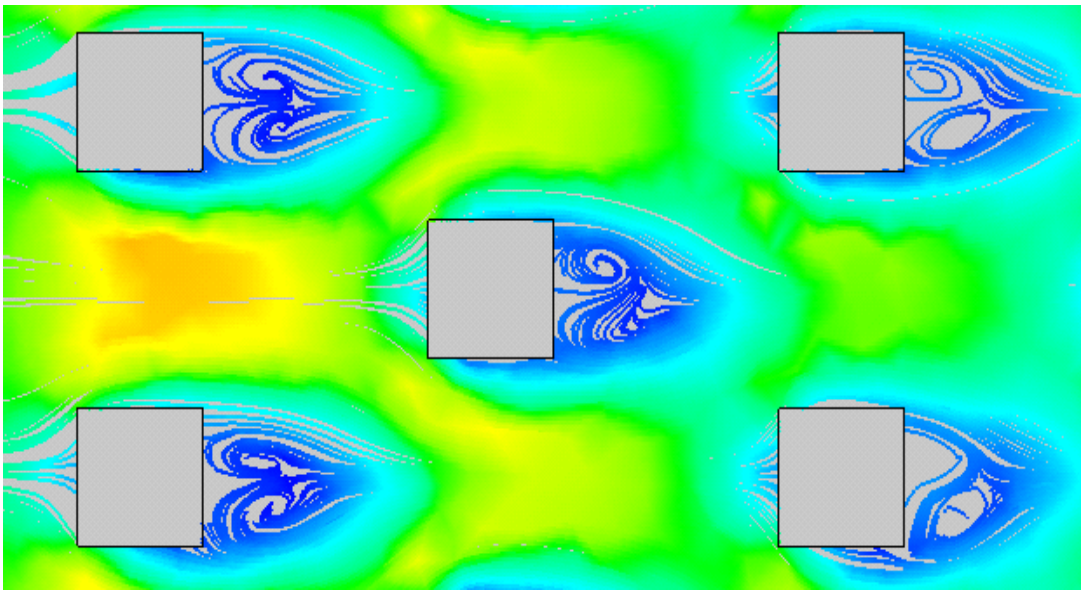

Figure: 18 Stream lines for m=0.01 kg/s (staggered arrangements)

By the observation of stream lines for staggered and in-line arrangement it has been found that swirls generation in case of staggered fins are more than in-line arrangement. Hence the heat transfer to the air will be higher in case of staggered fins.

4.3 Effect of recycling on thermal performance of solar collector

To investigate the effect of external recycle with fin fins attached on absorber plate, 196 square shape pin fins of 10 mm thickness (sides) and height 25 mm each were attached on absorber plate and reflux ratio was varied from 0 to 5 for mass flow rates of 0.01, 0.015 and 0.02 kg/s and its effects on collector efficiency and outlet air temperature are determined.

Table: 3 Improvement of collector performance with recycling, for t=10 mm and h=25 mm.

m	R	T_{pm} (K)	$T_{f,o}$(K)	η(%)	I(%)
0.01	0	337.09	301.66	45.60	0.00
	1	324.12	304.04	53.95	18.31
	2	318.93	305.03	57.29	25.63
	3	316.25	305.51	58.89	29.14
	4	315.38	305.68	59.49	30.46
	5	315.02	305.75	59.78	31.09
0.015					
	0	327.12	298.31	52.01	0.00
	1	317.12	299.87	59.61	14.63
	2	313.56	300.45	62.81	20.78
	3	311.89	300.74	64.21	23.48
	4	310.65	300.9	65.01	25.03
	5	310.32	300.96	65.41	25.78
0.02					
	0	321.95	296.37	56.30	0.00
	1	313.65	297.46	63.72	13.14
	2	310.15	297.92	66.7	18.47
	3	308.48	298.12	68.02	20.08
	4	307.40	298.23	68.71	22.04
	5	306.73	298.3	69.22	22.94

The improvement in collector efficiency I by operating with recycling is best illustrated by calculating the percentage increase in collector efficiency based on operating without recycling.

The device performance of pin fined attached single pass solar air heater with external recycle was investigated numerically. The advantages of pin fined attached solar air heater are to create turbulence intensity and enlarge the heat transfer area, and hence, the heat transfer efficiency is enhanced. The improvement in collector efficiencies of

Single- pass type solar air heaters with pin fins attached operating at same air flow rate, based on a single pass device without fins of the same working dimension, and were calculated and the results are presented in Table 3.

The collector efficiencies of both device, η and η_o, increase with air flow rate. The height and the thickness of the pin fin were varied from 0 to 45 mm and 0 to 30 mm respectively and results obtained are presented in Tables 2. The results show that to get optimum efficiency, the ratio of h/t should be high with lower mass flow rate, and should be comparatively low with higher mass flow rates. The optimum ratio of h/t for196 fins on absorber plate have been found as 4.5, 1.5-2, 1-1.2 with mass flow rates of 0.005, 0.01 and 0.02 kg/s respectively.

A comparison has been made between recycle type solar air heater with pin fins attached and longitudinal fins attached for almost same total cross section area of the fins, results show that efficiency of collector with pin fins

attached is 30% and 23% more than that of SAH with longitudinal fins attached for reflux ratio of 0 and 1 respectively, with mass flow rate 0.01 kg/s, and 22% and 19% more with mass flow rate of 0.02 kg/s for reflux ratio (R) of 0 and 1 respectively.

References

[1] Satcunanathan, S., and Deonarine, S., A two pass solar air heater, Solar Energy (1973), Vol. 15, Pages 41-49.

[2] Malhotra, A., Garg, H.P. and Rani, U., The effect of gap spacing on convective losses in flat plate collectors, Proceeding of National Solar Energy Convection, I.I.T Bombay (1979), Pages 52-56.

[3] Malhotra, A., Garg, H.P. and Rani, U., Minimizing convective heat losses in flat plate solar collectors, Solar Energy (1980), Vol. 25, Pages 521-526.

[4] Bevill, V.D. and Brandt, H., A solar energy collector for heating air, Solar Energy (1968), Vol. 15, Pages 19-29.

[5] Yeh HM, Tsai SW, Lin CS, A study of the separation efficiency in thermal diffusion column with a vertical permeable barrier. AIChE Journal (1986), Vol. 32 Pages 971–981.

[6] Yeh HM, Tsai SW, Chiang CL. Recycle effects on heat and mass transfer through a parallel-plate channel. AIChE Journal (1987), Vol. 33, Pages1743–1760.

[7] Ho CD, Yeh HM, Sheu WS. An analytical study of heat and mass transfer through a parallel-plate channel with recycle, International Journal of Heat and Mass Transfer (1998), Vol. 41, Pages 2589–2599.

[8] Ho CD, Yeh HM, Sheu WS. The influence of recycle on double-pass heat and mass transfer through a parallel-plate device, International Journal of Heat and Mass Transfer (1999), Vol. 42(9):1707–1722.

[9] Norris, R. H., Spofford, W. A: High-Performance Fins for Heat Transfer, Trans. ASME(1942), Vol. 64, Pages 489-496.

[10] Kays, W. M., Pin-Fin Heat-Exchanger Surfaces, Trans. ASME(1955), Vol. 77, Pages 471-483.

[11] Theoclitus, G., Heat-transfer and flow-friction characteristics on nine pin fin surfaces, J. Heat Transfer (1966), Pages 383-390.

[12] Sparrow, E. M., Ramsey, J. W., Heat transfer and pressure drop for a staggered wall-attached array of cylinders with tip clearance, Int. J. Heat Mass Transfer(1978), Vol. 21, Pages 1369-1377.

[13] VanFossen, G. J., Heat- Transfer Coefficients for Staggered Arrays of Short Pin Fins, Transactions of the ASME (1982), Vol. 104, Pages 268-274.

[14] Sparrow, E.M. and Molki, M. Effect of a Missing Cylinder on Heat Transfer and Fluid Flow in an Array of Cylinders in Cross-Flow, Inter. J. Heat Mass Transfer (1982), Vol.25, Pages 449-456.

[15] Metzger, D. E., Fan, C. D., Haley S. W., Effects of Pin Shape and Array Orientation on Heat Transfer and Pressure Loss in Pin Arrays, Trans. ASME (1984), Vol. 106, Pages 252-257.

[16] Babus'sHaq, F.R., Akintude, K., and Probert, D,S., Thermal Performance of a Pin-Fin Assembly, Int. J. Heat Fluid Flow (1995), Vol. 16, Pages 50-55.

[17] Li, Q. Chen, Zh., Flechtner, U., Warnecke, H.-J., Pressure drop and heat transfer of drop-shaped cylinder arrays, International Journal of Heat and Mass Transfer (1996), Vol. 68, Pages 1299-1302.

[18] Chen, Z., Li, Q., Meier, D., Warnecke, H. J., Convective heat transfer and pressure loss in rectangular ducts with drop-shaped pin fins, Heat and Mass Transfer (1997), Vol. 33, Pages 219-224.

[19] Li, Q., Chen, Zh., Flechtner, U., Warnecke, H.-J., Heat transfer and pressure drop characteristics in rectangular channels with elliptic pin fins, Int. J. Heat Fluid Flow (1998), Vol. 19, Pges 245-250.

[20] Yeh, J. J., Chuy, M. K., Heat Transfer of Staggered Pin Fin Arrays, Graduate Student Conference, Carnegie Mellon University, Pittsburgh, PA (1998).

[21] Maveety, J.G., Jung, H. H., Design of an optimal pin fin heat sink with air impingement cooling, Int. Commun. Heat Mass Transfer (2000), Vol.27 pages 229-240.

[22] Camci, C., Uzol, O., Elliptical pin fins as an alternative to circular pin fins for gas turbine blade cooling applications, ASME paper 2001-GT-0180.

[23] Issa, J., Ortega, A., Experimental Measurements of the Flow and heat Transfer of a Square Jet Impinging on an Array of Square Pin Fins, Proceedings to IMECE 2002, ASME Int. Engineering Congress & Exposition, New Orleans, LA.

[24] Short, E. B, Raad, P. E. and Price, D. C., Performance of Pin Fin Cast Aluminium Coldwalls, Part 1: Friction Factor Correlations, J. of Thermo physics and Heat Transfer (2003), Vol. 16, Pages 389-396.